Oikos

OIK-04458

Griffith, A. B. 2017. Perturbation approaches for integral projection models. – Oikos doi: 10.1111/oik.04458

Supplementary material

Appendix 1–7 (this file)

R-codes in separate files

Appendix 1

Table A1. Published articles using at least one of the five perturbation approaches described in the text (out of 173 total articles examined). Only articles that examined the response of asymptotic population growth to changes in life history vital rates are included.

	Approach				
Study	**1**	**2**	**3**	**4**	**5**
Aikens and Roach 2014					✓
Bassar et al. 2013			✓		
Bruna et al. 2014	✓				
Bruno et al. 2011		✓			
Childs et al. 2003		✓			
Childs et al. 2004		✓			
Chung et al. 2015		✓			✓
Coulson 2012					✓
Coulson et al. 2011					✓
Coulson et al. 2010					✓
Cursach et al. 2013		✓			
Dahlgren and Ehrlén 2009		✓			
Dahlgren et al. 2011		✓			
Dahlgren et al. 2014				✓	
Dalgleish et al. 2011		✓			
Dauer and Jongejans 2013	✓	✓			
Easterling et al. 2000	✓				
Elderd and Miller 2016					✓
Ellner and Rees 2006		✓			
Ellner and Schreiber 2012		✓			
Ferrer-Cervantes et al. 2012		✓			
Ford et al. 2015		✓			✓
Hegland et al. 2010		✓			
Hesse et al. 2008					✓
Isaza et al. 2016	✓				✓
Jacquemyn et al. 2010				✓	
Jansen et al. 2012		✓			
Jongejans et al. 2011		✓			
Kolb 2012	✓				
Kolb et al. 2010		✓			
Kuss et al. 2008		✓			
Li et al. 2015			✓		
Li et al. 2013			✓		

Li et al. 2011				✓		
Lubben et al. 2009						✓
Metcalf et al. 2009						✓
Miller et al. 2009		✓				
Miller et al. 2012						✓
Olsen et al. 2016			✓			
Ozgul et al. 2010					✓	
Ozgul et al. 2012					✓	
Plard et al. 2015		✓				
Plard et al. 2016						✓
Pozo et al. 2016						✓
Ramula 2014			✓			
Raventos et al. 2015					✓	
Rees and Ellner 2009			✓			✓
Rees and Rose 2002		✓	✓			✓
Salguero-Gómez et al. 2012						✓
Schwartz et al. 2016		✓	✓			
Smallegange et al. 2014						✓
Ureta et al. 2012		✓	✓			
van der Meer et al. 2016			✓			
van Kleef and Jongejans 2014						✓
Vindenes et al. 2014					✓	
Wallace et al. 2013			✓			✓
Wilber et al. 2016						✓
Williams et al. 2010					✓	
Williams and Crone 2006						✓
Yau et al. 2014			✓			
Yule et al. 2013						✓
Zambrano and Salguero-Gómez 2014			✓			
Zuidema et al. 2010			✓			
	Total	10	29	4	7	23

Appendix 2 – Simulated data, vital rate models, and IPM construction

The simulated demographic data for both populations assume an annual pre-breeding census, where offspring survival is incorporated into overall reproductive contributions. 1000 individuals from each population were assigned unit-less sizes drawn from a normal distribution (Figure A1). Expected survival, future size, and fecundity values for each individual were determined by evaluating specified generalized linear models (GLMs), with population differences implemented as an intercept shift (Table A2). Specific future sizes for individuals were drawn from a normal distribution based on the evaluated mean future size, with size-independent standard deviations specified for each population (Population A = 2.5, Population B = 4). Specific survival and fecundity values for individuals were randomly drawn from binomial and Poisson distributions, respectively, using the GLM predictions as parameters. Offspring survival data (e.g. seedling establishment) for 200 individuals from each population were randomly drawn from a binomial distribution. Similarly, offspring size data for 200 individuals from each population were randomly drawn from a normal distribution.

Vital rates for IPMs were determined by refitting GLMs to this simulated dataset using MCMCglmm (Hadfield 2010) with appropriate error distributions and link functions (Table A3). The standard deviation of future sizes was estimated from the model residual variance^{½}. Uncertainty in parameter estimates was incorporated into IPMs by sampling from the parameter posterior distributions while evaluating regressions (1000 iterations; Elderd and Miller 2016). All modeling and analysis was conducted using R (version 3.2.3; R Core Team 2015).

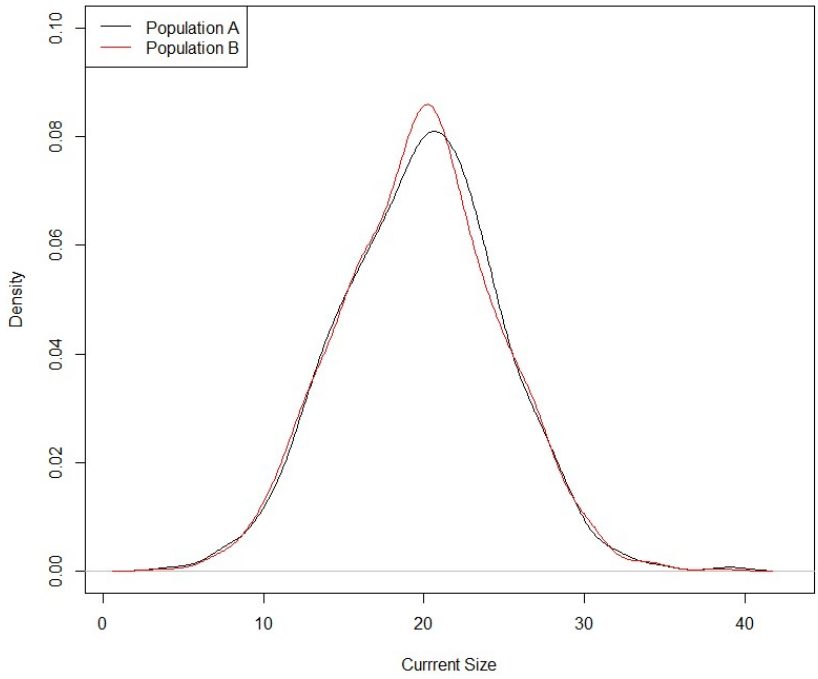

Figure A1. Size distributions of 1000 simulated individuals for each population. Unit-less sizes (z) were randomly drawn from a normal distribution (μ = 20, σ = 5).

Table A2. Generalized linear models (GLMs) were specified to assign expected survival (S), future mean size (G_μ), and fecundity (R) values for individuals.

$\text{logit}(S) =$	$-3.5 + 0.17z - 0.6Pop + 0.5e$
$G_\mu =$	$-3.5 + 1.6z - 0.017z^2 + 1.8Pop$
$\log(R) =$	$-4.5 + 0.25z + 0.1Pop + 0.5e$

z = Current size
e = Standard normal random value (environmental noise)
Pop = Population intercept shift: Population A = 1, Population B = -1

Table A3. Fitted vital rate model parameters for the simulated populations.

	Posterior mean	Lower 95% CI	Upper 95% CI
Future Size $G(z',z)$:			
Error Distribution: Gaussian			
Link: Identity			
Population A			
β_0	-2.102	-5.709	1.365
β_1	1.627	1.313	1.962
β_2	-0.017	-0.025	-0.011
Residual σ	2.440	2.263	2.630
Population B			
β_0	-6.110	-11.01	-1.228
β_1	1.612	1.151	2.095
β_2	-0.016	-0.027	-0.006
Residual σ	3.926	3.704	4.157
Survival $S(z)$:			
Error Distribution: Binomial			
Link: Logit (coefficients back-transformed)			
	Posterior mean	**Lower 95% CI**	**Upper 95% CI**
Population A			
β_0	-3.985	-4.741	-3.252
β_1	0.162	0.126	0.197
Population B			
β_0	-3.171	-3.905	-2.462
β_1	0.188	0.152	0.226
Fecundity $R(z)$:			
Error Distribution: Poisson			
Link: Log (coefficients back-transformed)			
	Posterior mean	**Lower 95% CI**	**Upper 95% CI**
Population A			
β_0	-4.215	-4.643	-3.801
β_1	0.250	0.233	0.266
Population B			
β_0	-4.568	-4.937	-4.197
β_1	0.251	0.236	0.266

Offspring survival OS:

Error Distribution: Binomial

Link: Logit (coefficients back-transformed)

	Posterior mean	Lower 95% CI	Upper 95% CI
Population A			
β_0	-2.570	-3.073	-2.045
Population B			
β_0	-2.027	-2.477	-1.602

Offspring mean size $OG(z')$:

Error Distribution: Gaussian

Link: Identity

	Posterior mean	Lower 95% CI	Upper 95% CI
Population A			
β_0	18.906	18.763	19.044
Residual σ	1.018	0.919	1.126
Population B			
β_0	16.207	15.908	16.492
Residual σ	2.144	1.941	2.369

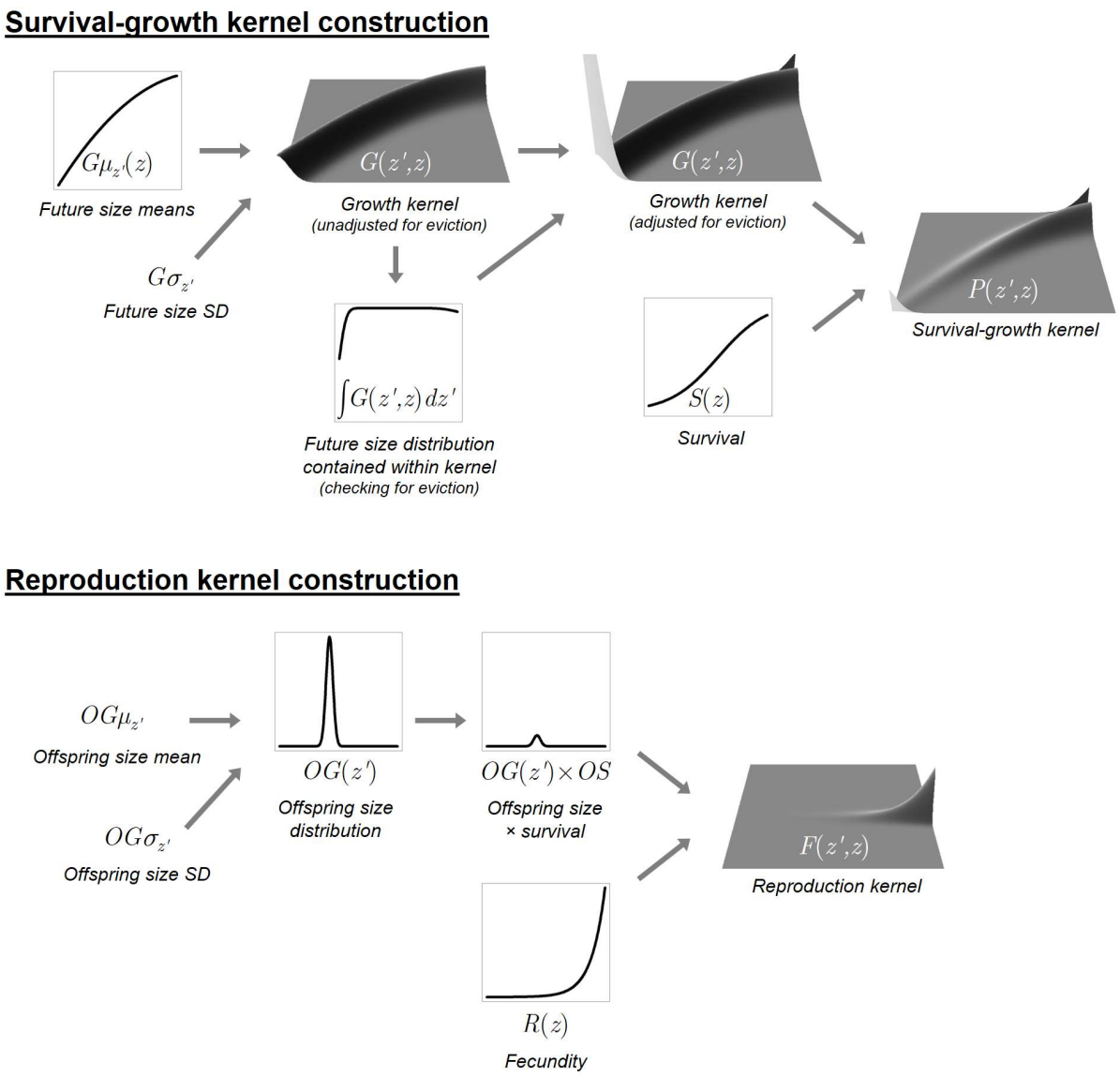

Figure A2. Conceptual IPM construction processes using continuous functions (data shown depict Population A). Note that this process is largely theoretical and the actual construction process in this case was based on functions/kernels discretized into 200 size classes.

Discretized Survival-growth kernel construction

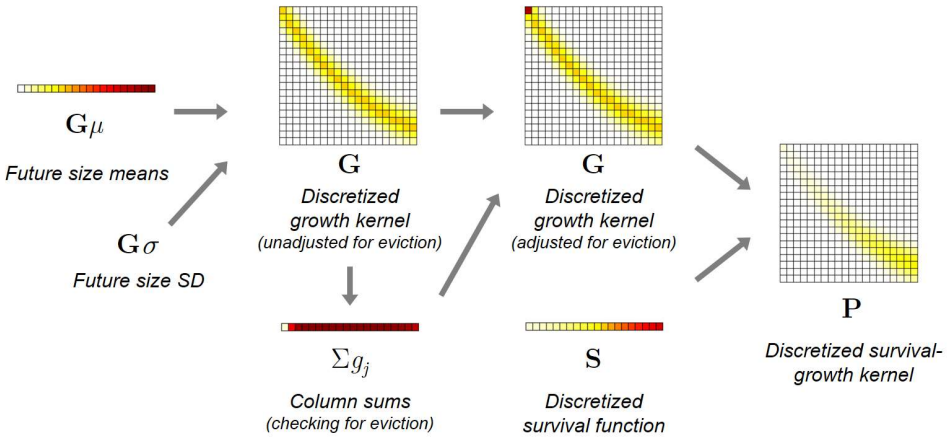

Discretized Reproduction kernel construction

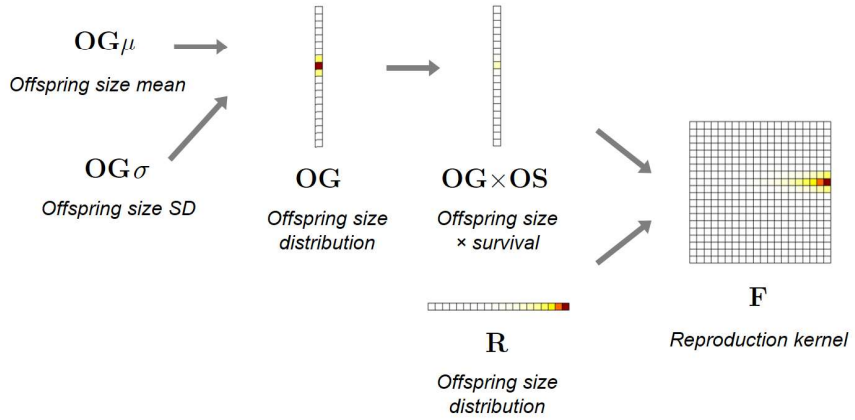

Figure A3. Conceptual IPM construction processes using discretized functions (data shown depict Population A). This example depicts 20 size classes (for clarity) compared to the 200 size classes used in the actual analysis, with the origin at the top-left (as in matrix models) compared to the bottom-left (more typical for IPMs).

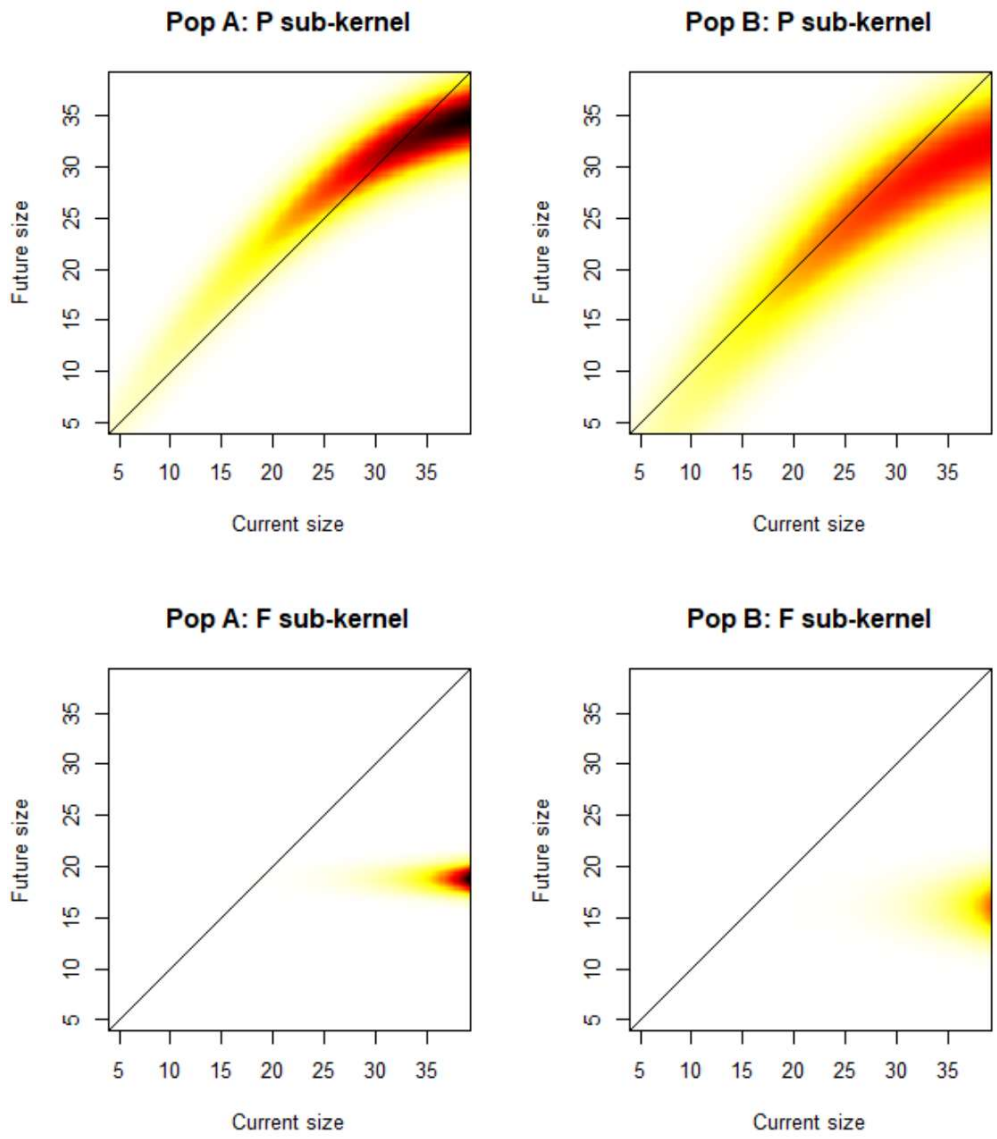

Figure A4. Survival-growth ($P(z',z)$) and reproduction ($F(z',z)$) kernels for each simulated population (unadjusted for size class eviction).

Appendix 3 – LTRE details

Life Table Response Experiment (LTRE) analysis examines how differences in vital rates among populations/treatments contribute to observed differences in λ by multiplying vital rate differences by their sensitivity value (Caswell 1989, 2001):

$$\lambda_A - \lambda_B \approx \sum_i \left[(a_{Ai} - a_{Bi}) \times \left(\frac{\partial \lambda_{\overline{AB}}}{\partial a_{\overline{AB}i}} \right) \right] = \sum_i \left[(a_{Ai} - a_{Bi}) \times sv_{a_{\overline{AB}i}} \right] \quad \text{(A1)}$$

where *A* and *B* represent different populations/treatments and $sv_{a_{\overline{AB}i}}$ is the sensitivity value of vital rate a_i at some midway value (typically the mean) between *A* and *B*. Midway models for each perturbation approach were created by averaging values of the two populations at the stage in the IPM construction process where the perturbation is applied (Table A4). For example, the midway model for Approach 2 was created by averaging elements in the discretized survival-growth (**P**) and reproduction (**F**) kernels across populations. Uncertainty in LTRE contributions for approaches 2-5 was incorporated by creating 1000 pairs of IPMs for Populations A and B by sampling from the posterior distributions of vital rate regressions. Differences in vital rates between populations for each iteration were multiplied by the corresponding sensitivity values of the midway model, which were based on the posterior means of vital rate parameters for each population. (Note that a slightly better LTRE approximation may be obtained by creating a unique midway model for each iteration; see Fig. A5.)

LTRE is considered to be a *retrospective* analysis because of its focus on observed differences (Caswell 2000) and has been applied in many cases to IPMs (e.g. Williams and Crone 2006, Ramula 2014, Bruna et al. 2014). While Eq. A1 represents a fixed design LTRE, it is also possible to examine across multiple levels of a random effect and express overall contributions in terms of variance explained (Brault and Caswell 1993).

Table A4. Description of midway model construction in the LTRE analyses for each perturbation approach. These are the methods used in the analyses in this paper, although it is certainly possible to justify alternative approaches for models used to evaluate sensitivities in LTRE analysis.

Perturbation approach	**LTRE midway model construction**[§]
(1) *Projection kernel*	Elements in **K** from each population were averaged to form the midway **K** matrix.
(2) *Additive sub-kernels*	Elements in **P** and **F** from each population were averaged and then added to produce the midway **K** matrix.
(3) V*ital rate functions*	Similar to above, but with elements in discretized vital rate vectors (**S**, **R**, **OS**) and matrices (**G**, **OG**) averaged across populations before being combined to produce midway **P**, **F**, and **K** matrices.
(4) *Vital rate regression predictions*	Vectors of size-dependent and size-independent (offspring) regression predictions and size residual standard deviations were averaged across populations prior to constructing IPM kernels.
(5) *Vital rate regression parameters*	Fitted model parameters were averaged across populations prior to evaluating regressions. Size residual standard deviations were averaged as above.

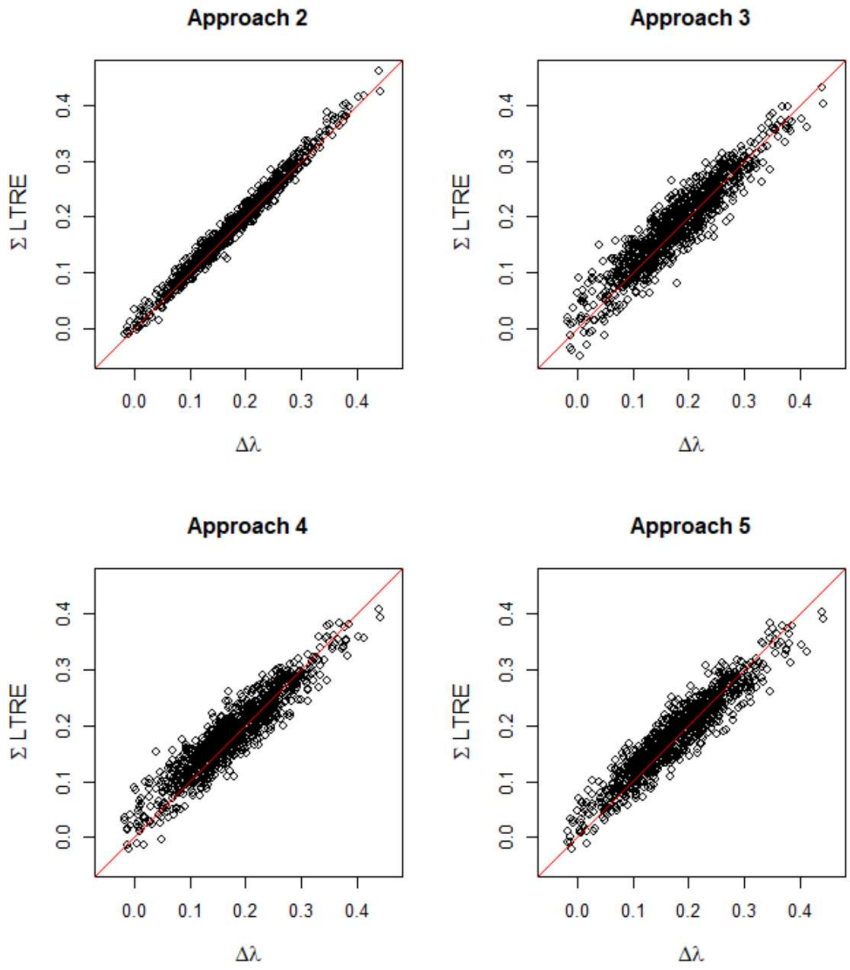

Figure A5. Summed LTRE contributions compared to differences in λ between populations for each iteration. LTRE is always an approximation (due to the use of a midway model between treatments/populations), and it is useful to examine the robustness of this approximation. It is likely that a slightly better approximation could have been achieved by creating a unique midway model for each iteration.

Appendix 4 – Elasticity value sums

A convenient property of the elasticity values of projection matrix elements is that they sum to one, due to the fact that λ is a homogeneous function of degree one with respect to all matrix elements (Caswell 2001). In other words, multiplying all the elements by x is the same as multiplying λ by x. However, this property does not necessarily apply to all lower-level vital rates that underlie and contribute to projection matrix elements. For example, if a matrix element associated with reproduction is the direct product of several vital rates (e.g. probability of reproducing × individual fecundity × offspring survival), then each vital rate will have the same elasticity value as the matrix element, which is itself a homogeneous function of degree one with respect to the underlying vital rates. Similarly, if a single vital rate underlies *all* matrix elements (e.g. adult survival in post-breeding models), then λ is a homogenous function of degree one with respect to this vital rate alone. In this case, the summed elasticity values for this single vital rate will invariantly equal one, with the overall sum of elasticity values being greater than unity (e.g. Franco and Silvertown 2004).

All of these properties can apply to elasticity values of discretized IPMs as well. Moreover, researchers using IPMs may also be interested in other perturbation targets, such as the mean and variance of the future size distribution and/or the vital rate regression parameters. Elasticity values for these parameters do not face constraints like those of matrix elements and can take on a broad range of values (e.g. a proportional change in the slope of the size regression can result in a *very* large proportional change in λ). In cases where elasticity values do not sum to one, it may be helpful to rescale values in order to facilitate comparisons across populations or species (Franco and Silvertown 2004, Jacquemyn et al. 2010).

Elasticity values and proportional compensation

From the text: *An interesting property of proportional compensation in IPMs is that the sum of all size transition elasticity values is zero (although discretization appears to cause the sum to approach zero as the matrix dimension increases). This appears to be due to the complete interdependence of elements within columns of* $\boldsymbol{G}$ *such that their collective influence is balanced. As such, this yields the satisfying result that the sum of elasticity values for size transitions and survival is the same as the survival-growth kernel.*

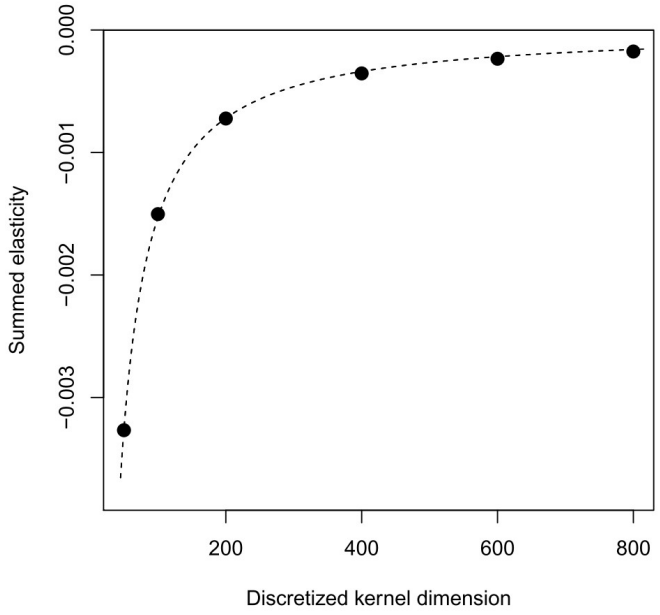

Figure A6. Summed elasticity values of the discretized size transition kernel (**G**) of different matrix dimensions. The dotted line is the negative of a 2 parameter power function fitted to the absolute values of the elasticity values.

Elasticity values and state variable

Table A5. Elasticity values (sums for Approaches 3 and 4) assuming different state variables. Shading indicates linear scaling within columns for each approach and thus represents relative values. See the text and Table 1 for description of terms.

Approach 3 – *Vital rate functions (proportional compensation)*				
	Diameter	***ln* Diameter**	**Area**	***ln* Area**
γ	0.165	0.170	0.163	0.170
ρ	-0.165	-0.168	-0.164	-0.168
s	0.799	0.774	0.812	0.775
r	0.201	0.226	0.188	0.225
$og > \mu$	0.045	0.055	0.037	0.055
$og < \mu$	-0.044	-0.054	-0.037	-0.054
os	0.201	0.226	0.188	0.225
Approach 4 – *Vital rate regression predictions*				
	Diameter	***ln* Diameter**	**Area**	***ln* Area**
$G\,\mu$	3.670	9.639	2.068	9.271
$G\,\sigma$	0.217	0.234	0.194	0.234
$S\,\mu$	0.813	0.792	0.823	0.792
$R\,\mu$	0.187	0.208	0.177	0.208
$OG\,\mu$	1.015	3.618	0.409	3.464
$OG\,\sigma$	0.035	0.054	0.022	0.054
$OS\,\mu$	0.187	0.208	0.177	0.208
Approach 5 – *Vital rate regression parameters*				
	Diameter	***ln* Diameter**	**Area**	***ln* Area**
$G\,\beta_0$	0.608	9.365	0.037	8.613
$G\,\beta_1$	5.845	30.48	2.600	28.54
$G\,\beta_2$	1.554	11.48	0.572	10.66
$G\,\sigma$	0.211	0.227	0.186	0.226
$S\,\beta_0$	0.862	2.489	0.419	2.391
$S\,\beta_1$	0.963	2.580	0.520	2.482
$R\,\beta_0$	0.783	3.356	0.241	3.212
$R\,\beta_1$	1.248	3.878	0.690	3.734
$OG\,\beta_0$	0.998	3.565	0.401	3.412
$OG\,\sigma$	0.035	0.054	0.022	0.054
$OS\,\beta_0$	0.310	0.348	0.291	0.349

Appendix 5 – Perturbation Approach 3 details

1. **Sensitivity formulae**

Below are the formulae for the analytical determination of sensitivity values for the discretized IPM vital rate functions of the simulated dataset. (See text and Table 1 for descriptions of terms and approach.) Note that for each equation, the terms multiplied by the corresponding sensitivity value of the overall kernel ($sv_{k_{ij}}$) depend on the specific construction of the kernel, in this case:

$$K(z', z) = S(z) \times G(z', z) + R(z) \times OS \times OG(z') \tag{A2}$$

(Eq. 1 in main text)

Note that for all vital rates below, elasticity values are calculated after determining sensitivity values using Eq. 3 in the main text:

$$ev_a = \frac{a}{\lambda} sv_a \tag{A3}$$

Size-dependent vital rates

Survival (s):

$$sv_{s_j} = \sum_i \left(sv_{k_{ij}} \times g_{ij} \right) \tag{A4}$$

(Eq. 9 in main text)

Growth (g):

Proportional compensation:

$$sv_{g_{ij}} = \left(sv_{k_{ij}} \times s_j\right) + \sum_{m \neq i} \left(-\frac{g_{mj}}{\sum_{p \neq i} g_{pj}} \times sv_{k_{mj}} \times s_j \right)$$

(A5)

(Eq. 13 in main text)

"Stasis-only" compensation (Zuidema and Franco 2001):

$$sv_{g_{ij}} = \left(sv_{k_{ij}} \times s_j\right) - \left(sv_{k_{jj}} \times s_j\right)$$

(A6)

Fecundity (r):

$$sv_{r_j} = \sum_i \left(sv_{k_{ij}} \times os \times og_i\right)$$

(A7)

(Eq. 11 in main text)

<u>*Size-independent vital rates*</u>

Vital rates associated with offspring are (in this case) independent of parent size. However, the influence of size-independent vital rates (e.g. os) on the overall projection kernel depends on the values of size-dependent vital rates (e.g. r). Thus, sensitivity and elasticity values calculated using this analytical approach are size-dependent, even if the vital rate of interest is not. This

makes biological sense given that prospective perturbation analysis examines hypothetical scenarios, e.g. increasing the survival of offspring produced by large individuals may have a strong influence on λ because large individuals produce more offspring.

Offspring Survival (os):

$$sv_{os_j} = \sum_i \left(sv_{k_{ij}} \times r_j \times og_i \right) \tag{A8}$$

Offspring Size (og):

$$sv_{og_{ij}} = \left(sv_{k_{ij}} \times r_j \times os \right) + \sum_{m \neq i} \left(-\frac{og_m}{\sum_{p \neq i} og_p} \times sv_{k_{mj}} \times r_j \times os \right) \tag{A9}$$

2. Compensation

The main article text presents an analytical approach to proportional compensation (Fig. A7, Eq. 13) using the *integrated sensitivity* framework of van Tienderen (1995). Details of this approach are described below, as well as a numerical approach that may more clearly highlight the concept of proportional compensation.

Numerical approach to proportional compensation

To calculate the sensitivity value for the ith element of column j in the size transition matrix $\mathbf{G}$ (g_{ij}), we can create a perturbed version of $\mathbf{G}$ ($\mathbf{G}_{perturbed}$) where g_{ij} is replaced by $g_{ij} + x$ (where x represents a small perturbation, e.g. 10^{-5}), and all other elements in the column are replaced by their corresponding values from the proportionally rescaled vector, $\mathbf{B}$:

$$\mathbf{B} = \begin{bmatrix} g_{1j} \\ \vdots \\ g_{nj} \end{bmatrix} \times \frac{\left(\sum_m g_{mj}\right) - g_{ij} - x}{\left(\sum_m g_{mj}\right) - g_{ij}} \tag{A10}$$

Assuming that within-column eviction has been accounted for (Williams et al. 2012), Σg_{mj} should equal 1, and Eq. A10 simplifies to

$$\mathbf{B} = \begin{bmatrix} g_{1j} \\ \vdots \\ g_{nj} \end{bmatrix} \times \frac{1 - g_{ij} - x}{1 - g_{ij}} \tag{A11}$$

The sensitivity value for g_{ij} would then be evaluated as

$$sv_{g_{ij}} \approx \frac{\Delta\lambda}{\Delta g_{ij}} = \frac{\lambda_{perturbed} - \lambda_{original}}{x} \tag{A12}$$

where $\lambda_{perturbed}$ is calculated from the IPM incorporating $\mathbf{G}_{perturbed}$. However, such a numerical approach for large matrices can be computationally taxing.

Analytical approach to proportional compensation

The same result can be achieved analytically by calculating van Tienderen's (1995) *integrated sensitivity* (*IS*), which explicitly accounts for covariance among matrix elements (following van Tienderen, the notation for Eq. A13-A15 uses linear indexing of matrix elements instead of row/column indexing, i.e. i and j refer to distinct matrix elements):

$$IS_{a_i} = sv_{a_i} + \sum_{j \neq i} b_{a_j|a_i} sv_{a_j} \tag{A13}$$

This approach adjusts the original sensitivity value of a projection matrix element (sv_{a_i}, assuming independence of matrix elements) by adding the influence of covariation with other matrix elements. sv_{a_i} is the sensitivity value of the jth matrix element (assuming independence of matrix elements) and $b_{a_j|a_i}$ is the partial derivative $\partial a_j / \partial a_i$. In this case, covariation among elements of $\mathbf{G}$ exists only within columns, and proportional compensation results in linear relationships between the perturbed and compensated elements within the same column (data not shown). Given this linearity we can express Eq. A13 as (van Tienderen 1995):

$$IS_{a_i} = sv_{a_i} + \sum_{j \neq i} \frac{V_{a_i a_j}}{V_{a_i}} sv_{a_j} \tag{A14}$$

where V_{a_i} is the variance in a_i, and $V_{a_i a_j}$ is the covariance between a_i and a_j. The proportional compensation described by Eq. A11 also results in predictable covariance/variance ratios for size transition probabilities within each column of $\mathbf{G}$, such that

$$\frac{V_{g_i g_j}}{V_{g_i}} = -\frac{g_j}{\sum_{\neq i} g_{col}} \tag{A15}$$

where the denominator is the sum of all elements in the column except g_i. Thus, we can fully apply van Tienderen's integrated sensitivity approach to the case of IPM size transition perturbations as follows (the notation reverts back to the row/column indexing as used in Eq. A11 to arrive at Eq. A5 from above (and Eq. 13 in main text):

$$sv_{g_{ij}} = \left(sv_{k_{ij}} \times s_j\right) + \sum_{m \neq i} \left(-\frac{g_{mj}}{\sum_{p \neq i} g_{pj}} \times sv_{k_{mj}} \times s_j \right)$$

The analytical approach of Eq. A5 (while still iterative) is much more computationally efficient than the numerical approach outlined in Eq. A10-A12 (although the latter remains useful for validation).

Comparison of compensation approaches

Although there are many possible approaches to distributing compensation among elements within a column, a relevant comparison here is between proportional compensation and the

'stasis-only' approach described by Zuidema & Franco (2001) and applied in a few cases to IPMs (Li et al. 2011, 2013, 2015). As described in the text, differences in assumptions between these two approaches point to the proportional approach as being most appropriate for IPMs. Important differences in the results of the two approaches strengthens this argument.

One consequence of placing the entire perturbation offset into stasis is an amplification of the original perturbation. For example, if size transitions resulting in growth (i.e. lower triangular elements) are most likely, then compensation via stasis would effectively decrease a transition that is relatively unfavorable to population growth (as stasis is at the low end of possible future sizes). This adds to the overall sensitivity values for growth due to increases to relatively favorable transitions combined with a decrease to a relatively unfavorable transition (Fig. A8A). Similarly, if retrogression is dominant, compensation that decreases stasis (which would be at the high end of possible future sizes) will further amplify the negative effect of increasing a transition resulting in retrogression (Fig. A8B). This outcome is also clearly evident when comparing elasticity values for the *Lupinus polyphyllus* pouplations (Fig. A9).

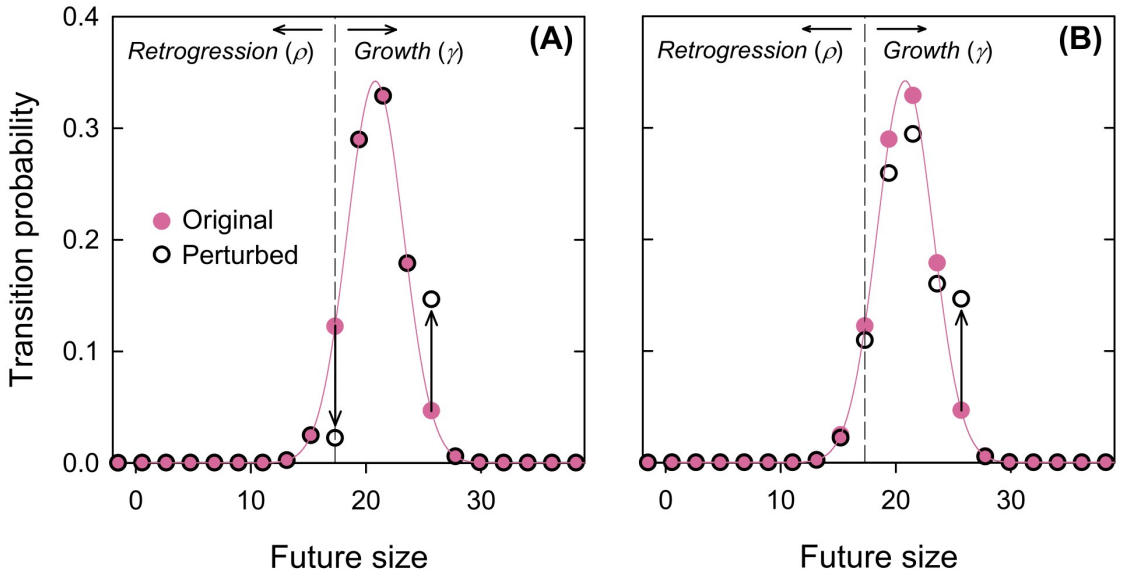

Figure A7. A comparison of (A) compensation via stasis and (B) proportional compensation for a 20×20 discretized IPM (the number of size classes was reduced from the analysis in the text for visual clarity). Filled circles represents the size transition probabilities for surviving individuals with a current size of 17.3 (i.e. single column). The example perturbation is an increase of 0.1 in the probability of transitioning from a size of 17.3 to 25.7 (up arrow), with open circles representing transition probabilities following the perturbation and counter perturbation.

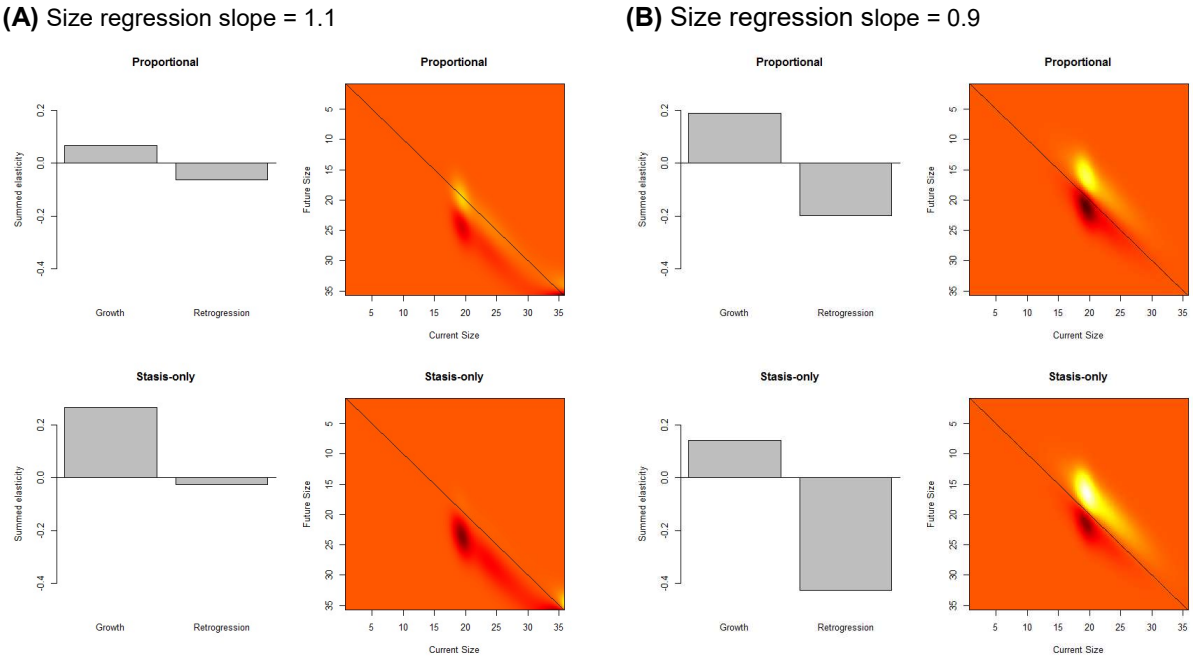

Figure A8. Elasticity values calculated using the proportional and stasis-only approaches to compensation. Analyses were performed for Population A with the size regression replaced with (A) $\mu = 1.1 \times z$ and (B) $\mu = 0.9 \times z$. Darker shading corresponds to higher values (consistent scale across panels) and color grayscale values are linear. Note that the y axis on kernels are reversed, and can thus be interpreted in the same manner as a projection matrix, with growth transitions found below the 1:1 line (stasis).

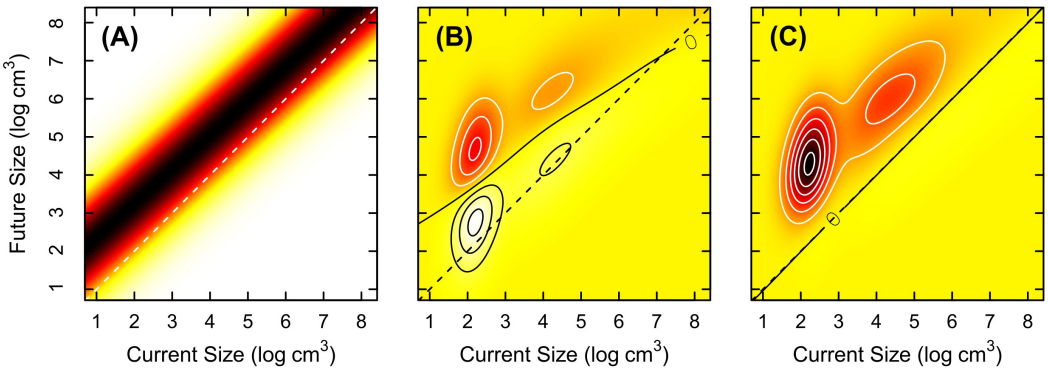

Figure A9. Example of sensitivity/elasticity amplification resulting from compensation via stasis only. (A) Size transition kernel ($G(z',z)$; shown without eviction adjustment) for the Southern population of *Lupinus polyphyllus*. Associated discretized elasticity kernels ($\mathbf{EV}_G$) calculated using (B) proportional compensation and (C) stasis-only compensation. Elasticity kernels include eviction adjustment (in this case simply implemented by rescaling columns to sum to one), which is evident in the slight bend of the zero isocline for panel B. Darker shading indicates higher values, and white and black contour lines in B and C surround positive and negative contributions, respectively. Color shading grayscale values are linear and use the same scale for B and C.

Appendix 6 –*Lupinus polyphyllus* vital rate models

The *Lupinus polyphyllus* data are a subset of 37 populations that were monitored across Finland where the species is invasive (see Ramula 2014 for details). Specifically, I compared two populations (Southern #13 and Central #7) spanning the annual transition from 2010 to 2011. These particular populations were chosen for comparison as they exhibited strongly different dynamics during this transition period, with individuals in the Southern population generally experiencing growth compared to relatively high probabilities of retrogression in the Central population. This is mirrored by λ values of 1.569 and 0.812 in the Southern and Central populations, respectively.

The vital rate models are the similar to the simulated dataset, with the added vital rate of flowering probability (fitted as binomial GLM with a logit link). Additionally, the mean future size regressions were fitted as first order linear models, and fecundity was fitted as a first order linear model with *ln*(seeds + 1) as the dependent variable (fecundity values were back-transformed after evaluating regressions). I chose to assume the absence of a seedbank, as the probability of seed dormancy/viability was estimated at the species level and thus did not differ among populations (hence the λ values here are slightly lower than those calculated by Ramula). To understand the differences in population dynamics between these two populations, I used LTRE analysis primarily based on Approach 3, but used Approach 4 to examine the contributions from differences in the parameters influencing the distribution of seedling sizes. Vital rate models for the two populations were fitted using MCMCglmm (Hadfield 2010), and the standard deviation for future size was estimated from the model residual variance^{½}.

Table A6. Fitted vital rate model parameters for the *Lupinus polyphyllus* populations.

Future Size $G(z',z)$:			
Error Distribution: Gaussian			
Link: Identity			
	Posterior mean	**Lower 95% CI**	**Upper 95% CI**
Southern #13			
β_0	1.468	0.892	2.048
β_1	0.894	0.754	1.026
Residual σ	1.020	0.892	1.161
Central #7			
β_0	0.763	0.065	1.448
β_1	0.807	0.678	0.941
Residual σ	0.922	0.785	1.095
Survival $S(z)$:			
Error Distribution: Binomial			
Link: Logit (coefficients back-transformed)			
	Posterior mean	**Lower 95% CI**	**Upper 95% CI**
Southern #13			
β_0	-4.534	-5.664	-3.54
β_1	1.346	1.034	1.727
Central #7			
β_0	-3.111	-4.396	-1.825
β_1	0.958	0.636	1.282
Flowering Probability $PF(z)$:			
Error Distribution: Binomial			
Link: Logit (coefficients back-transformed)			
	Posterior mean	**Lower 95% CI**	**Upper 95% CI**
Southern #13			
β_0	-14.896	-23.165	-9.125
β_1	2.630	1.553	4.140
Central #7			
β_0	-13.884	-22.601	-8.055
β_1	2.318	1.322	3.781

Fecundity $R(z)$:

Error Distribution: Gaussian

Link: Identity (seed data were *ln* + 1 transformed)

	Posterior mean	Lower 95% CI	Upper 95% CI
Southern #13			
β_0	4.618	3.889	5.348
β_1	0.092	-0.032	0.216
Central #7			
β_0	-1.924	-3.885	0.001
β_1	0.960	0.668	1.259

Offspring survival OS:

Error Distribution: Binomial

Link: Logit (coefficients back-transformed)

	Posterior mean	Lower 95% CI	Upper 95% CI
Southern #13			
β_0	-1.387	-1.790	-0.986
Central #7			
β_0	-3.553	-4.644	-2.693

Offspring mean size $OG(z')$

Error Distribution: Gaussian

Link: Identity

	Posterior mean	Lower 95% CI	Upper 95% CI
Southern #13			
β_0	1.921	1.85	1.994
Residual σ	0.421	0.372	0.476
Central #7			
β_0	1.888	1.822	1.955
Residual σ	0.355	0.312	0.404

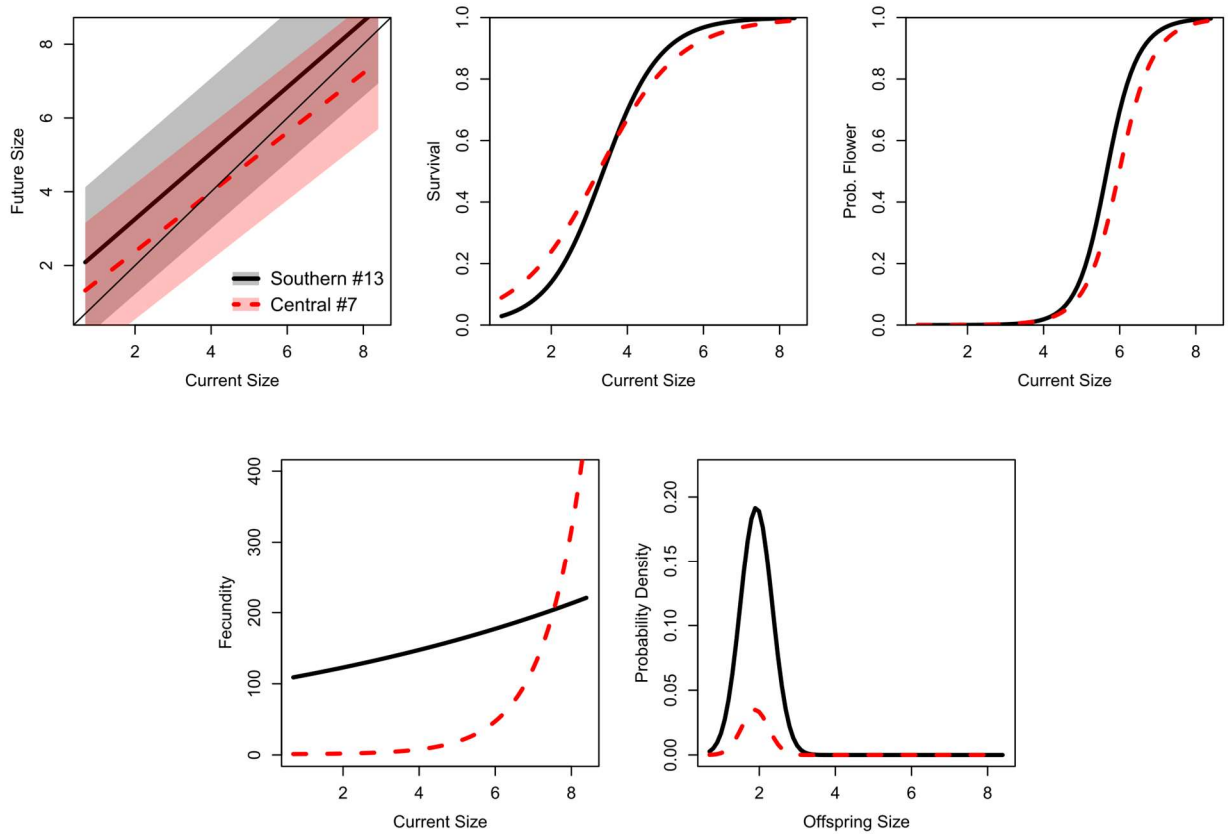

Figure A10. Vital rate regressions fit to both *Lupinus polyphyllus* populations. Shading around the mean future size regression lines indicates ± 2 SD. The probability densities for offspring size were multiplied by the probability of offspring survival and thus reflect the combined vital rates for offspring size and survival. All sizes are log cm^3.

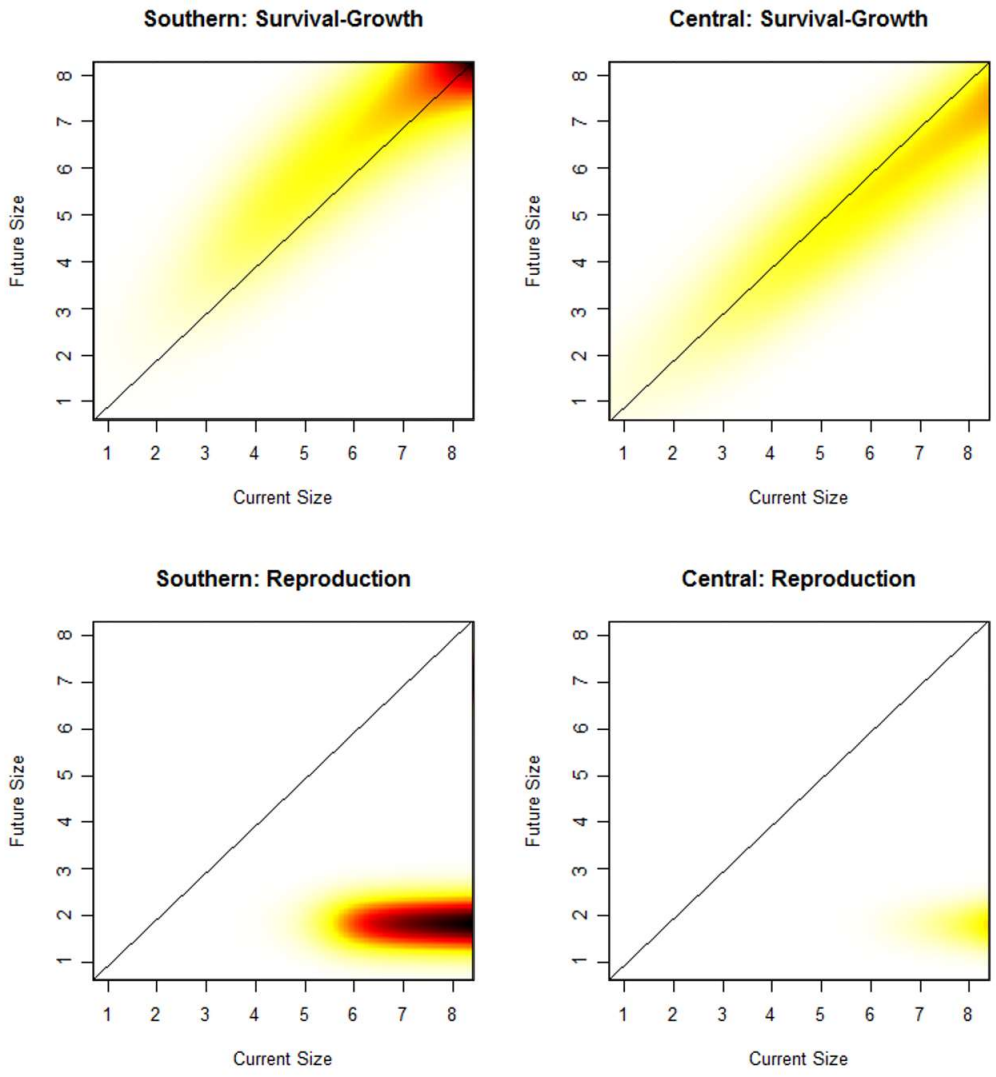

Figure A11. Survival-growth ($P(z',z)$) and Reproduction ($F(z',z)$) kernels for the *Lupinus polyphyllus* populations.

Appendix 7 – Description of included R scripts and data

Accompanying files

R Scripts

Approach 5 Templates.R Code templates for perturbing regression parameters for models fit using the *stats*, *lme4*, and *MCMCglmm* packages.

Fit Vital Rate Models.R Fits vital rate models for both populations using *MCMCglmm*. (Should be sourced by MAIN CODE.R, which specifies required objects.)

MAIN CODE.R This script contains all code for the analyses presented in the text, sourcing other .R files and loading .RData files where appropriate. Running/sourcing the script 'as is' will perform and plot all analyses using pre-fitted vital rate models and constructing 100×100 kernels with 1000 iterations. Vital rate models can easily be re-fit and kernel dimensions/iterations changed. Code for creating midway models, performing the LTRE analysis, and performing Approach 5 perturbations (regression parameters) are contained within this script.

Make Kernel IT.R This script is called by MAIN CODE.R to evaluate regressions and build IPM kernels while sampling from the model parameter posterior to generate multiple iterations.

Make Kernel.R This is essentially the same as Make Kernel IT.R, but it builds IPMs using the regression parameter means. (Perhaps more instructive and clearer to understand.)

MCMCglmm Predict Function.R Contains custom function used to predict fitted *MCMCglmm* models using new data.

MISC Functions.R Contains custom functions for plotting bar charts with error bars, copying data to the clipboard, and creating a white-yellow-red-black color palette that scales linearly in grayscale.

Perturbation Fucntions.R Contains functions to perform the analytical and numeric calculations of sensitivity and elasticity values described in the text and appendix for Approaches 1-4. (Approach 5 perturbation code is in MAIN CODE.R)

RData Files

Fitted Vital Rate Models.RData Contains fitted vital rate model objects. By default, MAIN CODE.R loads and uses these objects instead of re-fitting the models.

Kernels50.RData Includes pre-made kernel list objects that contain objects used to construct discretized 50×50 kernels based on mean vital rate parameters (i.e. not iterations sampled from posterior distributions).

Kernels100.RData Same as Kernels50.R, but with 100×100 kernels.

Kernels200.RData Same as Kernels50.R, but with 200×200 kernels.

Simulated Data.RData Contains the simulated dataset with the data frame `Data` containing information on existing individuals and the data frame `Estab` containing information on new recruits.

Information about perturbation functions

Most of the perturbation functions provided in the file 'Perturbation Approaches.R' require an input argument that is a list that contains objects used to construct the discretized IPM kernel. The list objects contained within 'Kernels50.RData', 'Kernels100.RData', and 'Kernels200.RData' adhere to this format and may include the following:

`n` Number of size classes in the discretized kernel (*length 1 numeric*)

`z`	Midpoint size value for each size class	(*length n numeric*)
`z.extend`	Extended size classes to correct for eviction	
`h`	Size class width	(*length 1 numeric*)
`K`	IPM projection kernel	(*n by n array*)
`P`	Survival-growth additive sub-kernel	(*n by n array*)
`F`	Reproduction additive sub-kernel	(*n by n array*)
`S`	Size-dependent survival	(*length n numeric*)
`G`	Size transition probabilities for surviving individuals	(*n by n array*)
`G.mu`	Size-dependent future size mean	(*length n numeric*)
`G.sig`	Size-independent future size SD	(*length 1 numeric*)
`R`	Size-dependent fecundity	(*length n numeric*)
`OS`	Size-independent offspring survival	(*length 1 numeric*)
`OG`	Size-independent offspring size probabilities	(*length n numeric*)
`OG.mu`	Size-independent offspring size mean	(*length 1 numeric*)
`OG.sig`	Size-independent offspring size SD	(*length 1 numeric*)

The lists `Kernel.Pop.A` and `Kernel.Pop.B` contain all of the objects above for each population and may therefore be passed to any of the functions contained within 'Perturbation Functions.R'. The lists `Kernel.Mid.1`, `Kernel.Mid.2`, `Kernel.Mid.3`, and `Kernel.Mid.4`, and `Kernel.Mid.5` contain objects used to build the 'midway' models shown in Fig. 3 and 4 and associated with the five different approaches. These models are constructed differently for each approach (Table A4), and thus their associated lists only contain relevant objects. For example, `Kernel.Mid.2` contains `K`, `P`, and `F` because the models were averaged at the level of the discretized sub-kernels ($\mathbf{P}$ and $\mathbf{F}$). The lists `Kernel.Pop.A`, `Kernel.Pop.B`, and `Kernel.Mid.5` also have objects that contain the posterior distributions for model parameters (`.Sol`) and residual variance (`.VCV`).

References

Aikens, M. L. and Roach, D. A. 2014. Population dynamics in central and edge populations of a narrowly endemic plant. - Ecology 95: 1850–1860.

Bassar, R. D. et al. 2013. Experimental evidence for density-dependent regulation and selection on Trinidadian guppy life histories. - Am. Nat. 181: 25–38.

Brault, S. and Caswell, H. 1993. Pod-specific demography of killer Whales (*Orcinus orca*). - Ecology 74: 1444–1454.

Bruna, E. M. et al. 2014. Effect of mutualist partner identity on plant demography. - Ecology 95: 3237–3243.

Bruno, J. F. et al. 2011. Impacts of aspergillosis on sea fan coral demography: modeling a moving target. - Ecol. Monogr. 81: 123–139.

Caswell, H. 1989. Analysis of life table response experiments I. Decomposition of effects on population growth rate. - Ecol. Model. 46: 221–237.

Caswell, H. 2000. Prospective and retrospective perturbation analyses: their roles in conservation biology. - Ecology 81: 619–627.

Caswell, H. 2001. Matrix population models: construction, analysis, and interpretation. - Sinauer Associates.

Childs, D. Z. et al. 2003. Evolution of complex flowering strategies: an age- and size-structured integral projection model. - Proc. R. Soc. B-Biol. Sci. 270: 1829–1838.

Childs, D. Z. et al. 2004. Evolution of size–dependent flowering in a variable environment: construction and analysis of a stochastic integral projection model. - Proc. R. Soc. Lond. B Biol. Sci. 271: 425–434.

Chung, Y. A. et al. 2015. Fungal symbionts maintain a rare plant population but demographic advantage drives the dominance of a common host. - J. Ecol. 103: 967–977.

Coulson, T. 2012. Integral projections models, their construction and use in posing hypotheses in ecology. - Oikos 121: 1337–1350.

Coulson, T. et al. 2010. Using evolutionary demography to link life history theory, quantitative genetics and population ecology. - J. Anim. Ecol. 79: 1226–1240.

Coulson, T. et al. 2011. Modeling effects of environmental change on wolf population dynamics, trait evolution, and life history. - Science 334: 1275–1278.

Cursach, J. et al. 2013. Demographic variation and conservation of the narrow endemic plant *Ranunculus weyleri*. - Acta Oecologica-Int. J. Ecol. 53: 102–109.

Dahlgren, J. P. and Ehrlén, J. 2009. Linking environmental variation to population dynamics of a forest herb. - J. Ecol. 97: 666–674.

Dahlgren, J. P. et al. 2011. Nonlinear relationships between vital rates and state variables in demographic models. - Ecology 92: 1181–1187.

Dahlgren, J. P. et al. 2014. Local environment and density-dependent feedbacks determine population growth in a forest herb. - Oecologia 176: 1023–1032.

Dalgleish, H. J. et al. 2011. Climate influences the demography of three dominant sagebrush steppe plants. - Ecology 92: 75–85.

Dauer, J. T. and Jongejans, E. 2013. Elucidating the population dynamics of Japanese knotweed using integral projection models. - Plos One 8: e75181.

Easterling, M. R. et al. 2000. Size-specific sensitivity: applying a new structured population model. - Ecology 81: 694–708.

Elderd, B. D. and Miller, T. E. X. 2016. Quantifying demographic uncertainty: Bayesian methods for integral projection models. - Ecol. Monogr. 86: 125–144.

Ellner, S. P. and Rees, M. 2006. Integral projection models for species with complex demography. - Am. Nat. 167: 410–428.

Ellner, S. P. and Schreiber, S. J. 2012. Temporally variable dispersal and demography can accelerate the spread of invading species. - Theor. Popul. Biol. 82: 283–298.

Ferrer-Cervantes, M. E. et al. 2012. Population dynamics of the cactus *Mammillaria gaumeri*: an integral projection model approach. - Popul. Ecol. 54: 321–334.

Ford, K. R. et al. 2015. The demographic consequences of mutualism: ants increase host-plant fruit production but not population growth. - Oecologia 179: 435–446.

Franco, M. and Silvertown, J. 2004. Comparative demography of plants based upon elasticities of vital rates. - Ecology 85: 531–538.

Hadfield, J. D. 2010. MCMC methods for multi-response generalized linear mixed models: the MCMCglmm R Package. - J. Stat. Softw. 33: 1–22.

Hegland, S. J. et al. 2010. Investigating the interaction between ungulate grazing and resource effects on *Vaccinium myrtillus* populations with integral projection models. - Oecologia 163: 695–706.

Hesse, E. et al. 2008. Life-history variation in contrasting habitats: flowering decisions in a clonal perennial herb (*Veratrum album*). - Am. Nat. 172: 196–213.

Isaza, C. et al. 2016. Demography of *Oenocarpus bataua* and implications for sustainable harvest of its fruit in western Amazon. - Popul. Ecol. 58: 463–476.

Jacquemyn, H. et al. 2010. Size-dependent flowering and costs of reproduction affect population dynamics in a tuberous perennial woodland orchid. - J. Ecol. 98: 1204–1215.

Jansen, M. et al. 2012. Strong persistent growth differences govern individual performance and population dynamics in a tropical forest understorey palm. - J. Ecol. 100: 1224–1232.

Jongejans, E. et al. 2011. Importance of individual and environmental variation for invasive species spread: a spatial integral projection model. - Ecology 92: 86–97.

Kolb, A. 2012. Differential effects of herbivory and pathogen infestation on plant population dynamics. - Plant Ecol. 213: 315–326.

Kolb, A. et al. 2010. Population size affects vital rates but not population growth rate of a perennial plant. - Ecology 91: 3210–3217.

Kuss, P. et al. 2008. Evolutionary demography of long-lived monocarpic perennials: a time-lagged integral projection model. - J. Ecol. 96: 821–832.

Li, S.-L. et al. 2011. Habitat-specific demography across dune fixation stages in a semi-arid sandland: understanding the expansion, stabilization and decline of a dominant shrub. - J. Ecol. 99: 610–620.

Li, S.-L. et al. 2013. Understanding the effects of a new grazing policy: the impact of seasonal grazing on shrub demography in the Inner Mongolian steppe. - J. Appl. Ecol. 50: 1377–1386.

Li, S.-L. et al. 2015. Mobile dune fixation by a fast-growing clonal plant: a full life-cycle analysis. - Sci. Rep. 5: 8935.

Lubben, J. et al. 2009. Parameterizing the growth-decline boundary for uncertain population projection models. - Theor. Popul. Biol. 75: 85–97.

Metcalf, C. J. E. et al. 2009. Seed predators and the evolutionarily stable flowering strategy in the invasive plant, *Carduus nutans*. - Evol. Ecol. 23: 893–906.

Miller, T. E. X. et al. 2009. Impacts of insect herbivory on cactus population dynamics: experimental demography across an environmental gradient. - Ecol. Monogr. 79: 155–172.

Miller, T. E. X. et al. 2012. Evolutionary demography of iteroparous plants: incorporating non-lethal costs of reproduction into integral projection models. - Proc. R. Soc. B-Biol. Sci. 279: 2831–2840.

Olsen, S. L. et al. 2016. From facilitation to competition: temperature-driven shift in dominant plant interactions affects population dynamics in seminatural grasslands. - Glob. Change Biol. 22: 1915–1926.

Ozgul, A. et al. 2010. Coupled dynamics of body mass and population growth in response to environmental change. - Nature 466: 482–U5.

Ozgul, A. et al. 2012. Population responses to perturbations: the importance of trait-based analysis illustrated through a microcosm experiment. - Am. Nat. 179: 582–594.

Plard, F. et al. 2015. Quantifying the influence of measured and unmeasured individual differences on demography. - J. Anim. Ecol. 84: 1434–1445.

Plard, F. et al. 2016. Des différences, pourquoi? Transmission, maintenance and effects of phenotypic variance. - J. Anim. Ecol. 85: 356–370.

Pozo, R. A. et al. 2016. Modeling the impact of selective harvesting on red deer antlers. - J. Wildl. Manag. 80: 978–989.

Ramula, S. 2014. Linking vital rates to invasiveness of a perennial herb. - Oecologia 174: 1255–1264.

Raventos, J. et al. 2015. Population viability analysis of the epiphytic ghost orchid (*Dendrophylax lindenii*) in Cuba. - Biotropica 47: 179–189.

R Core Team 2015. R: A language and environment for statistical computing. - R Foundation for Statistical Computing.

Rees, M. and Rose, K. E. 2002. Evolution of flowering strategies in *Oenothera glazioviana*: an integral projection model approach. - Proc. R. Soc. B-Biol. Sci. 269: 1509–1515.

Rees, M. and Ellner, S. P. 2009. Integral projection models for populations in temporally varying environments. - Ecol. Monogr. 79: 575–594.

Salguero-Gómez, R. et al. 2012. A demographic approach to study effects of climate change in desert plants. - Philos. Trans. R. Soc. B-Biol. Sci. 367: 3100–3114.

Schwartz, L. M. et al. 2016. Using integral projection models to compare population dynamics of four closely related species. - Popul. Ecol. 58: 285–292.

Smallegange, I. M. et al. 2014. Correlative changes in life-history variables in response to environmental change in a model organism. - Am. Nat. 183: 784–797.

Ureta, C. et al. 2012. Assessing extinction risks under the combined effects of climate change and human disturbance through the analysis of life-history plasticity. - Perspect. Plant Ecol. Evol. Syst. 14: 393–401.

van der Meer, S. et al. 2016. Recent range expansion of a terrestrial orchid corresponds with climate-driven variation in its population dynamics. - Oecologia 181: 435–448.

van Kleef, H. H. and Jongejans, E. 2014. Identifying drivers of pumpkinseed invasiveness using population models. - Aquat. Invasions 9: 315–326.

van Tienderen, P. H. 1995. Life-cycle trade-offs in matrix population models. - Ecology 76: 2482–2489.

Vindenes, Y. et al. 2014. Effects of climate change on trait-based dynamics of a top predator in freshwater ecosystems. - Am. Nat. 183: 243–256.

Wallace, K. et al. 2013. Re-evaluating the effect of harvesting regimes on Nile crocodiles using an integral projection model. - J. Anim. Ecol. 82: 155–165.

Wilber, M. Q. et al. 2016. Integral projection models for host–parasite systems with an application to amphibian chytrid fungus. - Methods Ecol. Evol. 7: 1182–1194.

Williams, J. L. and Crone, E. E. 2006. The impact of invasive grasses on the population growth of *Anemone patens*, a long-lived native forb. - Ecology 87: 3200–3208.

Williams, J. L. et al. 2010. Testing hypotheses for exotic plant success: parallel experiments in the native and introduced ranges. - Ecology 91: 1355–1366.

Williams, J. L. et al. 2012. Avoiding unintentional eviction from integral projection models. - Ecology 93: 2008–2014.

Yau, A. J. et al. 2014. Fishery management priorities vary with self-recruitment in sedentary marine populations. - Ecol. Appl. 24: 1490–1504.

Yule, K. M. et al. 2013. Costs, benefits, and loss of vertically transmitted symbionts affect host population dynamics. - Oikos 122: 1512–1520.

Zambrano, J. and Salguero-Gómez, R. 2014. Forest fragmentation alters the population dynamics of a late-successional tropical tree. - Biotropica 46: 556–564.

Zuidema, P. A. and Franco, M. 2001. Integrating vital rate variability into perturbation analysis: an evaluation for matrix population models of six plant species. - J. Ecol. 89: 995–1005.

Zuidema, P. A. et al. 2010. Integral projection models for trees: a new parameterization method and a validation of model output. - J. Ecol. 98: 345–355.